SCIENTIFIC REPORTS

OPEN

Antiferromagnetic Kondo lattice compound $CePt_3P$

Jian Chen[1,2], Zhen Wang[1], Shiyi Zheng[1], Chunmu Feng[1], Jianhui Dai[3] & Zhu'an Xu[1,4,5]

Received: 28 September 2016
Accepted: 29 December 2016
Published: 03 February 2017

A new ternary platinum phosphide $CePt_3P$ was synthesized and characterized by means of magnetic, thermodynamic and transport measurements. The compound crystallizes in an antiperovskite tetragonal structure similar to that in the canonical family of platinum-based superconductors APt_3P (A = Sr, Ca, La) and closely related to the noncentrosymmetric heavy fermion superconductor $CePt_3Si$. In contrast to all the superconducting counterparts, however, no superconductivity is observed in $CePt_3P$ down to 0.5 K. Instead, $CePt_3P$ displays a coexistence of antiferromagnetic ordering, Kondo effect and crystalline electric field effect. A field-induced spin-flop transition is observed below the magnetic ordering temperature T_{N1} of 3.0 K while the Kondo temperature is of similar magnitude as T_{N1}. The obtained Sommerfeld coefficient of electronic specific heat is $\gamma_{Ce} = 86$ mJ/mol·K^2 indicating that $CePt_3P$ is a moderately correlated antiferromagnetic Kondo lattice compound.

The interplay among spin, charge and orbital degrees of freedom in transition metal compounds has triggered enormous research interests in condensed matter physics and material science. For a large family of layered 3*d* electron superconductors (SCs) such as the copper oxides[1] and iron pnictides[2], the spin fluctuations caused by strong 3*d* electron correlations play a vital role in the unconventional superconductivity. Besides these 3*d* transition metal systems, several platinum-based SCs exhibit remarkably rich physical properties and therefore have also attracted considerable attention, partly owing to the moderately strong spin-orbit coupling of the platinum 5*d* electrons. The most prominent example is the heavy fermion noncentrosymmetric (NCS) SC $CePt_3Si$, in which exotic superconductivity is observed below $T_c = 0.75$ K[3]: an admixture of spin-singlet and spin-triplet pairing symmetry, nodal gap structure and huge upper critical field ($B_{c2} \approx 4$ T)[4]. The delicate interplay between the cerium 4*f* and the platinum 5*d* electrons places this material on the border of the magnetic quantum critical point (QCP) but still in the antiferromagnetic (AFM) gound state, rendering the role of inversion symmetry unclear[5]. Among a series of filled skutterudite MT_4X_{12} (M = rare-earth or alkaline-earth metals, T = transition metals and X = P, As, Sb and Ge) with the cubic space group $Im\bar{3}$ (No. 204), $PrPt_4Ge_{12}$ was reported to exhibit time-reversal symmetry breaking from zero-field μSR measurements[6]. As a result of the unexpectedly high transition temperature $T_c = 7.9$ K and the moderately enhanced Sommerfeld coefficient $\gamma = 76$ mJ/mol · K^2, $PrPt_4Ge_{12}$ has been extensively studied and multiband superconductivity has been proposed based on the analysis of the photoemission spectroscopy[7] as well as the magnetic penetration depth[8]. Moreover, SrPtAs is recently reported to crystallize in a hexagonal structure ($P6_3/mmc$, No. 194) with weakly coupled PtAs layers forming a honeycomb lattice[9]. The peculiar locally NCS structure within PtAs layer together with a strong spin-orbit coupling demonstrates SrPtAs as an attractive material to explore superconductivity with a spontaneous static magnetic field B_s[10].

It is interesting that among the platinum-based superconductors, the newly reported family of APt_3P (A = Ca, Sr and La) shares the structural similarity with that of iron pnictides[11]. These compounds crystallize in a tetragonal structure with space group $P4/nmm$ (No. 129) with stacking in the order of A-Pt_6P-A along the c-axis. The distorted antiperovskite Pt_6P octahedral unit alternates within the ab plane, forming an antipolar pattern. The $z \rightarrow -z$ inversion operation is thus preserved. Due to the structural distortion, the platinum atoms take two different sites as Pt(I) and Pt(II) so that the Pt(II) and P atoms form a Pt_2P layer resembling the FeAs layer in the iron-based superconductors. Of course, the structure of APt_3P is also somewhat similar to that of $CePt_3Si$, but the latter is actually isotypic to the NCS compound $CePt_3B$ with the space group $P4mm$ (No. 99)[3]. The corresponding Pt_6Si unit has the polar structure under this space group leading to the absence of inversion symmetry,

[1]Department of Physics and State Key Laboratory of Silicon Materials, Zhejiang University, Hangzhou 310027, China. [2]Zhejiang University of Water Resources and Electric Power, Hangzhou 310018, China. [3]Department of Physics, Hangzhou Normal University, Hangzhou 310036, China. [4]Zhejiang California International NanoSystems Institute, Zhejiang University, Hangzhou 310058, China. [5]Collaborative Innovation Center of Advanced Microstructures, Nanjing 210093, China. Correspondence and requests for materials should be addressed to J.C. (email: chenjian123@zju.edu.cn) or Z.X. (email: zhuan@zju.edu.cn)

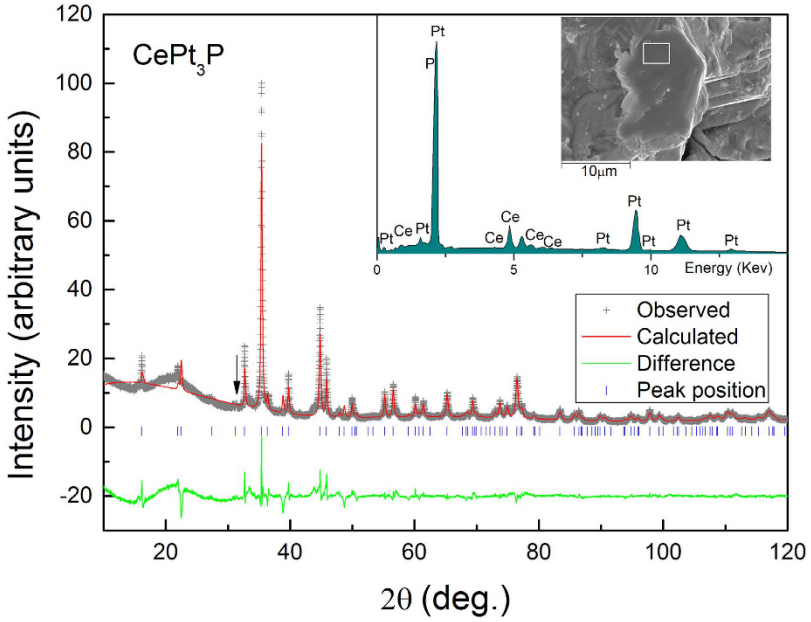

Figure 1. Rietveld refinement of the polycrystalline $CePt_3P$ XRD pattern. Arrow marks an impurity phase which might be PtP_2. Inset shows a typical energy-dispersive x-ray spectrum with electron beams focused on the selected area of the as-grown sample.

	SrPt3P	CaPt3P	LaPt3P	$CePt_3P$
a (Å)	5.8094	5.6673	5.7597	5.7123
c (Å)	5.2822	5.4665	5.4736	5.4679
$z_{Pt(II)}$	0.1409	—	0.1459	0.1582
z_P	0.7226	—	0.7691	0.8310
T_c/T_N (K)	8.4	6.6	1.5	3.0 (T_{N1})
				1.9 (T_{N2})
ρ_0 ($\mu\Omega\cdot$cm)	140	—	32	688
γ_0 (mJ/mol$\cdot$K^2)	12.7	17.4	1.5	86

Table 1. Comparisons of physical parameters among the APt_3P family with A = Sr, Ca, La and Ce. Atomic positions: A (0, 0, 0), Pt(I) (1/4, 1/4, 1/2), Pt(II) (0, 1/2, $z_{Pt(II)}$), P (0, 1/2, z_P). Note that data of Sr and Ca are taken from ref. 11.

different from the antipolar structure in APt_3P. Noticeably, the APt_3P family shows a significant variation of T_c, i.e., $T_c = 8.4$ K, 6.6 K and 1.5 K for A = Sr, Ca and La, respectively. It was reported theoretically that spin-orbit coupling (SOC) effect is significant in $LaPt_3P$ but negligible in $CaPt_3P$ and $SrPt_3P$[12–14]. The origin of significantly enhanced T_c in $SrPt_3P$ is still debatable. It was suggested to be due to a possible dynamic charge-density-wave (CDW)[12]. However, a theoretical work by Zocco *et al.* indicated SOC could strongly renormalize the electron-phonon coupling of $SrPt_3P$ and thus enhance the electronic density of states near the Fermi level[15]. Moreover, several theoretical works claimed that the CDW instability could not be reproduced in $SrPt_3P$[13,14]. The centrosymmetric (CS) compounds APt_3P reported so far do not involve the 4*f* electrons. The interplay between strong 4*f* electron correlation and superconductivity of 5*d* electrons in the APt_3P family remains an open issue.

In this paper, we report our successful synthesis of such a candidate compound $CePt_3P$ in the platinum-based phosphides APt_3P family. We performed systematic measurements of the physical properties including the magnetic susceptibility, magnetization, specific heat and electrical resistivity. However, no evidence of superconductivity is observed down to 0.5 K in $CePt_3P$, in contrast to other APt_3P compounds. Instead, the compound displays the rich physics involving the coexistence of magnetic ordering, Kondo coherence as well as crystalline electric field (CEF) effect. We shall discuss these properties and highlight the delicate 4*f*-5*d* interplay in this system.

Results and Discussion

Figure 1 shows the Rietveld refinement of the XRD pattern of polycrystalline $CePt_3P$ samples. Almost all peaks can be well indexed with the tetragonal structure with the space group *P*4/*nmm* (No. 129), except for a tiny peak of an impurity phase around 31.4° which might be PtP_2. The result of the Rietveld refinement[16] shows a good convergence: $R_{wp} = 13.4\%$, $S = 3.3$. The refined lattice parameters of $CePt_3P$ are $a = 5.7123(7)$ Å and $c = 5.4679(6)$ Å as listed in Table 1. The room temperature XRD patterns of $LaPt_3P$ are also refined with $R_{wp} = 14.9\%$, $S = 2.7$

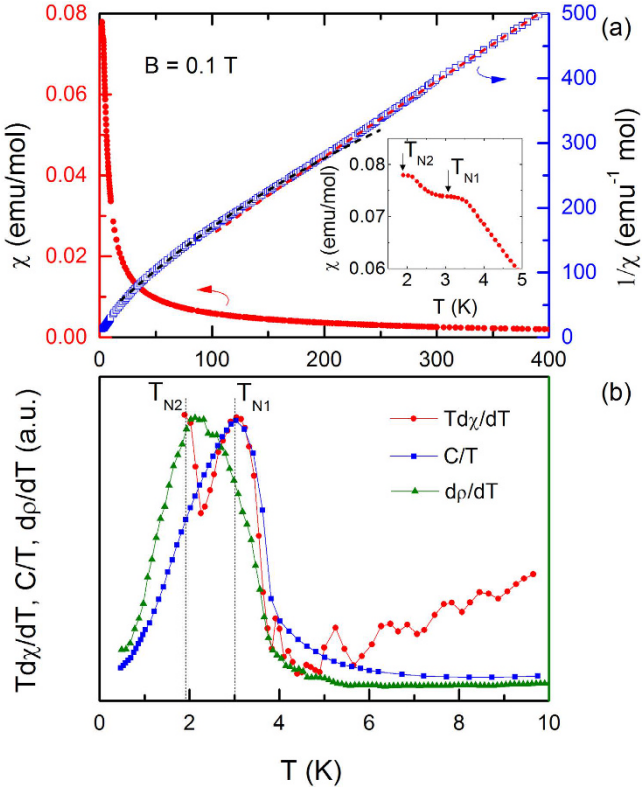

Figure 2. (**a**) Temperature dependence of magnetic susceptibility, χ, and inverse magnetic susceptibility, $1/\chi$, of $CePt_3P$ measured under magnetic field $B = 0.1$ T on the left and right axis, respectively. Two dashed lines show the Curie-Weiss fit for $T > 200$ K and $T < 100$ K, respectively. Inset: enlarged plot of χ at $T < 5$ K. (**b**) The AFM transition temperature T_{N1} and T_{N2} determined from the derivative susceptibility $Td\chi/dT$, specific heat $C(T)/T$ and derivative resistivity $d\rho/dT$ (The complete data of specific heat and resistivity will be shown in the following figures).

(data not shown). The refined lattice parameters of $LaPt_3P$ are $a = 5.7597(3)$ Å and $c = 5.4736(3)$ Å. For comparison, the lattice parameters of the other APt_3P compounds are also provided in Table 1. One can see obviously that a of $CePt_3P$ is smaller, while c is larger, compared with the lattice parameters of $SrPt_3P$. Due to the lanthanide contraction, both of a and c of $CePt_3P$ are smaller than those of $LaPt_3P$. From the EDS measurements, the molar ratio is Ce:Pt:P = (1.0 ± 0.1):(3.2 ± 0.2):(0.7 ± 0.2) for $CePt_3P$ and La:Pt:P = (1.0 ± 0.1):(2.6 ± 0.1): (0.8 ± 0.1) for $LaPt_3P$. The actual chemical compositions are close to the nominal ones, while there seems a deficiency on the P site for both $CePt_3P$ and $LaPt_3P$.

The temperature-dependent molar magnetic susceptibility $\chi(T) = M/H$ and inverse magnetic susceptibility $1/\chi(T)$ of $CePt_3P$ measured at $H = 1000$ Oe are presented in Fig. 2(a). $\chi(T)$ obeys a modified Curie-Weiss law above 200 K, $\chi = \chi_0 + \ell/(T - \theta)$. χ_0 is a temperature independent susceptibility from the core diamagnetism, the van Vleck and Pauli paramagnetism, ℓ is the Curie constant and θ is the Weiss temperature. The relatively large absolute value of $\theta = -28.3$ K may be attributed to the hybridization of the 4f electronic states with the conduction band[17]. The derived effective moment $\mu_{eff} = 2.52\mu_B$ is almost equal to that of a free Ce^{3+} ion, indicating the trivalent Ce ion and well localized moment of Ce-4f^1 electrons at high temperature. χ_0 is in the magnitude order of 10^{-3}. For $T < 100$ K, a change of the slope of $1/\chi(T)$ can be clearly observed and the fitting parameters are $\mu_{eff} = 2.11\mu_B$, and $\theta = -15.3$ K. Here the change of the slope and the decreased value of μ_{eff} can be ascribed to the CEF effect. With decreasing temperature, $\chi(T)$ increases and shows a round peak around 3.0 K. Upon further cooling, another anomaly is observed near our base temperature. Two magnetic transition temperatures are determined from the peaks of derivative susceptibility $Td\chi/dT$ as $T_{N1} = 3.0$ K and $T_{N2} = 1.9$ K (seen from Fig. 2(b)). Considering the negative Weiss temperature, the first anomaly marks the AFM ordering below T_{N1} which is compatible with the magnetization measurement (discussed below). While the second anomaly is attributed to a spin-reorientation. A similar phenomenon was observed in CeNiAsO[18]. Further experimental studies, especially neutron diffraction measurement on single crystals of $CePt_3P$, are necessary to clarify the magnetic structure at low temperature.

The isothermal magnetization $M(B)$ of $CePt_3P$, measured in the B-sweep mode containing both field-up and down loops, is displayed in Fig. 3(a). In the AFM ordering state, $M(B)$ displays a linear field dependence when $B < 2.0$ T, but undergoes a weak step-like increase around 3.0 T. This anomaly, which is ascribed to a field-induced metamagnetic transition (MMT), can be independently determined to be $B_m = 3.0$ T by the peak in dM/dB curve (inset to Fig. 3(a)) and the hump in $\rho(B)$ curve (Fig. 3(b)) measured at $T = 2$ K. The expected hysteresis around B_m is not observed and such absence of hysteresis around MMT was also reported in the single-crystalline samples

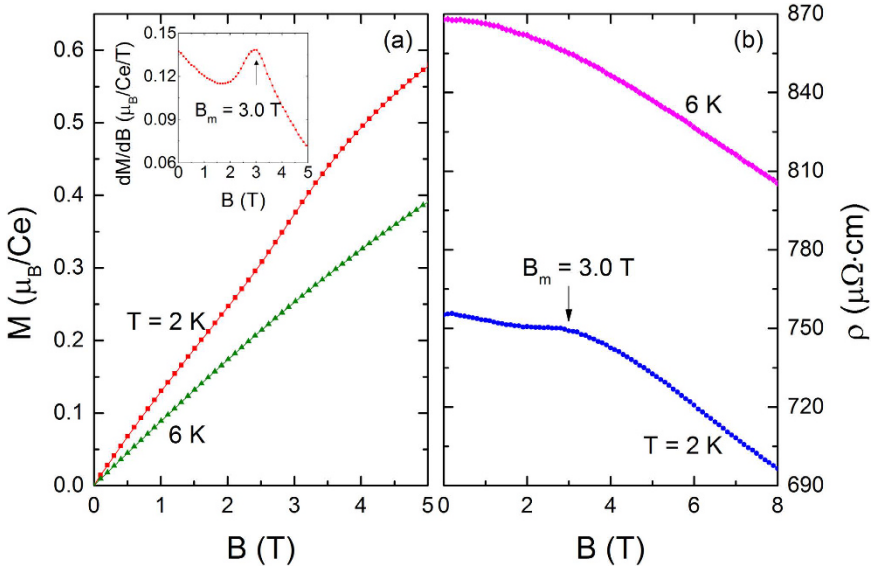

Figure 3. (**a**) Field dependence of the magnetization $M(B)$. (**b**) Resistivity ρ of $CePt_3P$ vs. B measured at $T = 2$ and 6 K. Inset to (**a**) displays the derivative of the magnetization with respect to the field dM/dB for $T = 2$ K.

$CeAuSb_2$[19] and $YbNiSi_3$[20]. No hysteresis in resistivity is observed for $CePt_3P$ in this magnetic field range either. Note that the $M(B)$ curve does not show a saturation trend in the highest field limit and the value $M \sim 0.6\mu_B$ at $B = 5$ T is much lower than the theoretical value of $2.14\mu_B$ for the saturated moment of free Ce^{3+} ions which is probably due to the CEF effect. Figure 3(b) shows the isothermal resistivity versus the applied field. ρ decreases monotonously with increasing magnetic field at $T = 6\,\mathrm{K} > T_{N1}$. Whereas at $T = 2\,\mathrm{K} < T_{N1}$, a hump around $B_m = 3.0$ T is added to the decreasing trend. This feature is compatible with the MMT observed in the magnetization measurement.

The specific heats of $CePt_3P$ and $LaPt_3P$ divided by T, $C(T)/T$, are plotted in the main panel of Fig. 4(a) in a semi-logarithm scale. At room temperature, $C(T)$ saturates to about 135 and 140 J/mol · K for La and Ce compound, respectively, which are, within an acceptable error range, compatible with the classical Dulong-Petit law $3NR$ with $N = 5$ and $R = 8.31$ J/mol · K, where R is the universal gas constant. The specific heat $C(T)$ of $LaPt_3P$ is typical for nonmagnetic metals since no typical anomaly can be observed at high temperature. At low temperature, the specific heat of $LaPt_3P$ is dominated by the electronic and phonon contributions for $T < \Theta_D/10$, therefore, it can be fitted to a power law $C/T = \gamma_{La} + \beta_{La}T^2$ over 10–20 K (data not shown). Here Θ_D is the Debye temperature, and γ_{La} and β_{La} denote the coefficients of the electronic and phonon contributions, respectively. It should be noted that there is a small jump around 1 K in the specific heat of $LaPt_3P$ which should correspond to a superconducting transition though it is too small to observe in Fig. 4.

In the paramagnetic region above the magnetic transition, the specific heat of $CePt_3P$ can be expressed as

$$C = \gamma_{Ce}T + \beta_{Ce}T^3 + C_{Sch}, \quad (1)$$

where the coefficients γ_{Ce} and β_{Ce} are of electronic and phonon contributions of $CePt_3P$, respectively, while C_{Sch} describes the Schottky anomaly item. A linear T^2-dependence is clearly seen in C/T vs T^2 plot for temperature below 20 K (see inset to Fig. 4(a)). The derived Sommerfeld coefficient is $\gamma_{Ce} = (86 \pm 1)$ mJ/mol · K^2. The value is moderately enhanced by a factor of 57 compared with that of $LaPt_3P$ where $\gamma_{La} = (1.5 \pm 0.1)$ mJ/mol · K^2, manifesting the correlation effect contributed from the Ce-4*f* electrons. Therefore, $CePt_3P$ is a Kondo lattice compound due to the strong 4*f* electron correlation and moderate effective $4f-5d$ hybridization. Note that γ_{La} for $LaPt_3P$ derived here is slightly smaller but still in the same magnitude order with that obtained in ref. 11. The reported phonon coefficients are in reasonable agreement with each other: $\beta_{Ce} = 0.98(1)$ mJ/mol · K^4 for $CePt_3P$ and $\beta_{La} = 0.94(1)$ mJ/mol · K^4 for $LaPt_3P$, indicating similar phonon contributions. The Debye temperature Θ_D estimated by using $\Theta_D = (12\pi^4 NR/5\beta)^{1/3}$ is (215 ± 1) K for $CePt_3P$ and (218 ± 1) K for $LaPt_3P$, implying that the above analysis is quite self-consistent.

The Ce-4*f* contribution to the specific heat of $CePt_3P$ is then deduced by subtracting the measured specific heat of the nonmagnetic isostructural reference sample $LaPt_3P$ from the total specific heat of $CePt_3P$, i.e., $C_{4f} = C_{Ce} - C_{La}$. The result is shown in the main panel of Fig. 4(b), plotted as C_{4f}/T vs T in a logarithmic scale. The Schottky anomaly, which is visible as a broad peak centered around 90 K in C_{4f}/T curve, should be caused by the excitations between different CEF levels. The Schottky anomaly with three Kramers doublets (one doublet ground state and two excited doublets) for Ce^{3+} ion with $j = 5/2$ experiencing a tetragonal crystal-field potential can be expressed by refs 21,22

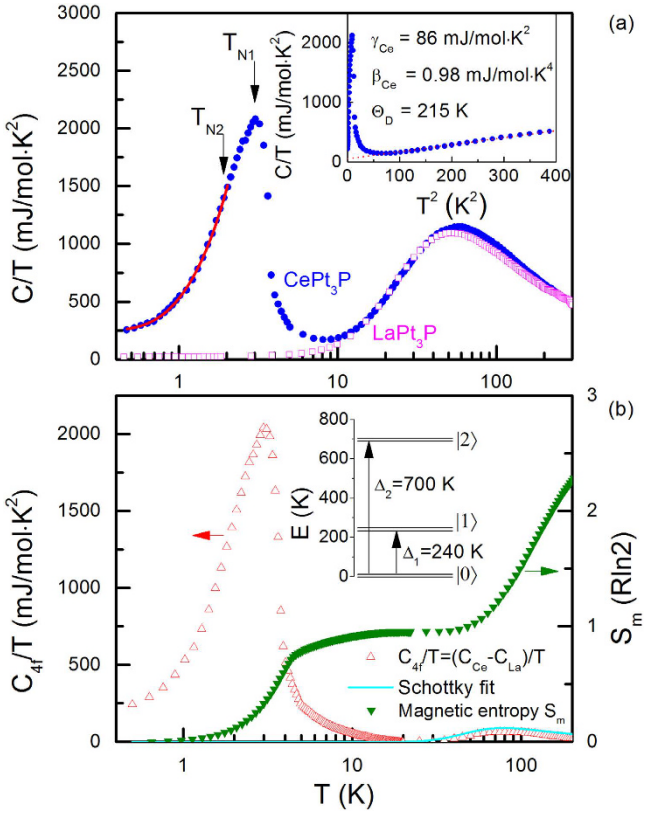

Figure 4. (**a**) Specific heat divided by temperature, C/T, versus log$T$. The solid symbols are for $CePt_3P$, while the open symbols represent the non-magnetic compound $LaPt_3P$. The solid line is a fit to Eq. 5 for $T \leq 1.9$ K. (**b**) The Ce-4*f* contribution, C_{4f}/T, and the magnetic entropy, S_m, on the left and right axis, respectively, measured at zero magnetic field plotted in a logarithmic temperature scale for $T = 0.4$–200 K. The solid line shows the Schottky anomaly contribution C_{Sch}. Inset to (**a**) shows C/T versus T^2 together with the fitting parameters for $CePt_3P$ (see the text): the Sommerfeld coefficient γ_{Ce}, β_{Ce} and the Debye temperature Θ_D. The dashed line is a linear fit in the temperature range $T = 10$–20 K. Inset to (**b**) displays the schematic sketch of CEF energy levels for Ce^{3+} ion in $CePt_3P$.

$$C_{Sch} = \frac{R}{g_0 + g_1 \exp(-\Delta_1/T) + g_2 \exp(-\Delta_2/T)} \times \{g_0 g_1 (\Delta_1/T)^2 \times \exp(-\Delta_1/T) + g_0 g_2 (\Delta_2/T)^2 \exp(-\Delta_2/T) + g_1 g_2 [(\Delta_2 - \Delta_1)/T]^2 \exp[-(\Delta_1 + \Delta_2)/T]\}. \quad (2)$$

Here $g_i = 2$ is the degeneracy of the ith doublet state and Δ_i is the energy difference between the ground state and the i-th excited state (see the schematic sketch drawn in the inset of Fig. 4(b)). Eq. 2 is applied to C_{4f}/T of $CePt_3P$ over a temperature range of 50–130 K. The derived CEF energy differences are $\Delta_1 = (20.9 \pm 0.1)$ meV (~(240 ± 1) K) and $\Delta_2 = (60.9 \pm 0.3)$ meV (~(700 ± 3) K). This result may explain the slope change in $1/\chi(T)$ curve as well as the broad hump in both ρ_{mag} and S. Furthermore, the large value of Δ_1 is consistent with the reduced effective Ce moment below 100 K. The magnetic entropy gain S_m is calculated by integrating C_{4f}/T over T and plotted on the right axis in Fig. 4(b). One can see that S_m reaches about 0.51*R*ln2 at T_{N1} and *R*ln2 is recovered at ~50 K, indicating that the ground state with the AFM ordering of Ce^{3+} moments is Kramers two-fold degenerate. The plateau over the temperature range of $T = 10$–30 K indicates that the first excited CEF level is far above T_{N1}. S_m reaches *R*ln4 at ~150 K and increases substantially above the Schottky anomaly. For a Kondo lattice, the Kondo temperature can be estimated by the magnetic entropy at T_N via ref. 23

$$S_m(\xi) = R \ln [1 + \exp(-\xi)] + \xi \frac{\exp(-\xi)}{1 + \exp(-\xi)}, \quad (3)$$

where $\xi = T_K/T_N$. The yielded T_K is about (6.1 ± 0.1) K for $CePt_3P$.

At low temperature, C_{4f}/T shows a pronounced λ-shape peak at $T_{N1} = 3.0$ K, implying a second-order phase transition. The expected jump in specific heat is $\delta C_{4f}|_{T=T_{N1}} \sim 6$ J/mol · K. A slight slope change in C_{4f}/T is also observed around $T_{N2} = 1.9$ K, consistent with the low-temperature anomaly observed in aforepresented $\chi(T)$

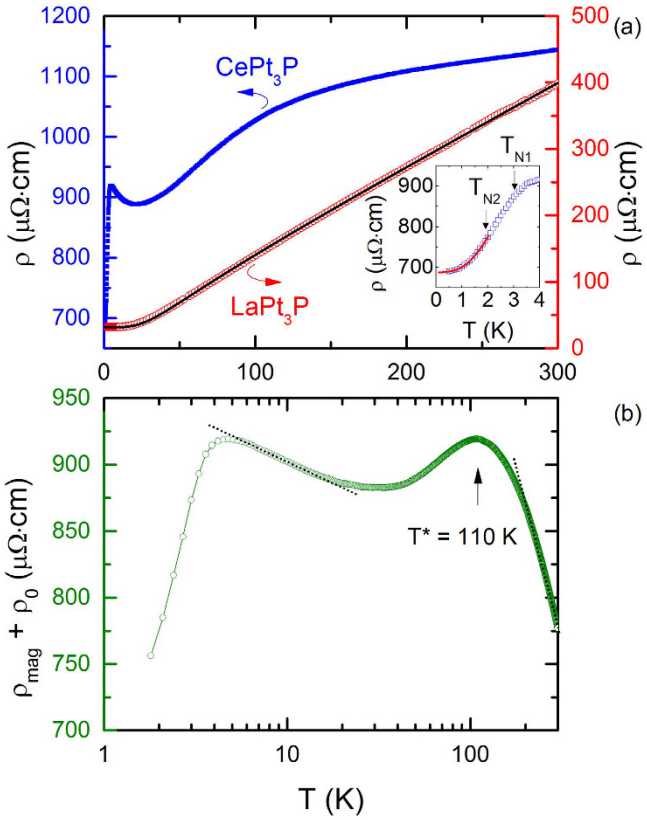

Figure 5. Transport properties as a function of temperature. (**a**) $\rho(T)$ of $CePt_3P$ and $LaPt_3P$ in a linear temperature scale. The solid line is a fit to the Bloch-Grüneissen-Mott formula (Eq. 6). (**b**) The magnetic contribution to the electrical resistivity of $CePt_3P$, ρ_{mag}, versus log$T$. The dashed lines display linear fits in the low and the high temperature regions, respectively. Inset to (**a**) plots a fit to Eq. 8 below $T \leq 1.9$ K.

curve. Based on the mean-field theory of Besnus *et al.*[24] and Bredl *et al.*[25], the specific heat jump $\delta C_{|T=T_N}$ is related to the Kondo temperature T_K by the following formula

$$\delta C(\zeta) = \frac{6R}{\psi'''\left(\frac{1}{2}+\zeta\right)}\left[\psi'\left(\frac{1}{2}+\zeta\right)+\zeta\psi''\left(\frac{1}{2}+\zeta\right)\right]^2. \tag{4}$$

Here $\zeta = (T_K/T_N)/2\pi$, ψ denotes the digamma function and ψ', ψ'' and ψ''' are the first three derivatives of ψ. Then the Kondo temperature can be also estimated by applying Eq. 4, obtaining a ratio of $T_K/T_{N1} = 0.88$, or $T_K \sim (2.7 \pm 0.1)$ K. Therefore, based on both magnetic entropy and specific heat jump, it is reasonable to estimate $T_K \sim 2$–6 K in this compound.

In the magnetically ordered state, the AFM spin-wave spectrum follows a dispersion relation of $\varepsilon_k = \sqrt{\Delta^2 + Dk^2}$. Here ε_k is the excitation energy, Δ is the gap in the spin-wave spectrum, and D is the spin-wave stiffness. The phonon contribution, $\beta_{Ce}T^3$ item, can be subtracted from the total specific heat C as $\Delta C = C - \beta_{Ce}T^3$. At low temperature, ΔC is described by the following expression[26,27]:

$$\Delta C(T) = \gamma_0 T + A_C \Delta^4 \sqrt{\frac{T}{\Delta}}\left[1 + \frac{39}{20}\left(\frac{T}{\Delta}\right) + \frac{51}{32}\left(\frac{T}{\Delta}\right)^2\right]\exp(-\Delta/T), \tag{5}$$

where the coefficient A_C is proportional to D^{-3}. Fitting the specific heat below T_{N2} (solid line in Fig. 4(a)) gives the fitting parameters $\gamma_0 = 247$ mJ/mol · K^2, $\Delta = 2.6$ K, and $A_C = 67.5$ mJ/mol · K^4. The considerably enhanced zero-temperature Sommerfeld coefficient γ_0 is about 3 times of γ_{Ce} obtained in the paramagnetic state, indicating the formation of moderate-heavy quasiparticles in the antiferromagnetically ordered state. It is worthwile noting that the obtained spin-wave gap Δ is of the order of magnitude often found in cerium intermetallics with AFM ground states[17].

The temperature variation of the electrical resistivity of $CePt_3P$, $\rho(T)$, is plotted in Fig. 5(a). The resistivity at room temperature is $\rho_{300K} = 1140\ \mu\Omega \cdot$ cm, a value rather typical for the Ce-based Kondo compounds with narrow f-band[28]. The resistivity decreases with decreasing temperature and exhibits two features. A broad hump around 110 K reflects the 4f-electron contribution via Kondo scattering from different CEF levels[21,22]. At low temperature, a pronounced peak in $\rho(T)$ around 3 K is directly visible, indicating the AFM ordering phase below $T_{N1} = 3.0$ K. Above T_{N1}, ρ increases in a minus logarithmic temperature manner over $T = 5$–20 K, reflecting the Kondo-type

scattering. Further evaluation of $\rho(T)$ requires information of the phonon contribution which could be taken from the homologous and isostructural analog, $LaPt_3P$. The $\rho(T)$ of $LaPt_3P$, which is also presented in Fig. 5(a), can be well described by a Bloch-Grüeneisen-Mott (BGM) relation:

$$\rho(T) = \rho_0 + 4R\Theta_R\left(\frac{T}{\Theta_R}\right)^5 \int_0^{\Theta_R/T} \frac{x^5 dx}{(e^x - 1)(1 - e^{-x})} - KT^3, \tag{6}$$

where ρ_0 is the residual resistivity due to lattice defects, the second term denotes electron-phonon scattering, and the third one accounts for the contribution due to Mott's *s-d* interband electron scattering. A least square fitting of the BGM formula to the experimental data over the temperature range 2–300 K leads to the following parameters: $\rho_0 = 32\ \mu\Omega\cdot$m, $\Theta_R = 160$ K, $R = 1.25\ \mu\Omega\cdot$cm/K, and $K = 4.1\times10^{-8}\ \mu\Omega\cdot$cm/K^3. Note that the residual resistivity ρ_0 is smaller than that in ref. 11. The parameter Θ_R is usually considered as an approximation of the Debye temperature Θ_D in spite of some contribution due to electron-electron correlations in Θ_R[29]. Θ_D yielded from the specific heat data is 218 K which is in accordance with Θ_R from the resistivity data. $LaPt_3P$ exhibits simple metallic behavior as we expected, without the characteristic features due to the interplay of Kondo and CEF effects in $CePt_3P$ mentioned above.

In order to analyze the magnetic contribution to the electrical resistivity of $CePt_3P$, it is reasonable to assume that the phonon contribution in this compound can be properly approximated by that in $LaPt_3P$, $\rho_{ph} = \rho(La) - \rho_0(La)$, so we have

$$\rho_{mag}(Ce) + \rho_0(Ce) = \rho(Ce) - \rho_{ph}. \tag{7}$$

The temperature dependence of $\rho_{mag} + \rho_0$ derived in this way is presented in Fig. 5(b) in a semilogarithmic scale. As a distinct feature in a Kondo lattice system, a pronounced broad hump centered at $T^* = 110$ K become obvious in ρ_{mag} curve, which could be ascribed to the Kondo scattering from different CEF levels. According to Cornut and Coqblin[21], this maximum provides an estimate of the CEF splitting energy scale ~200 K of Ce-4f^1 state with $j = 5/2$. On the other hand, as temperature is decreased, ρ_{mag} increases in a logarithmic scale, as shown as the dotted lines in Fig. 5(b) above $T > 200$ K and between 5–20 K, respectively. Following the theoretical predictions of Cornut and Coqblin[21], the logarithmic slopes c_K^{LT} and c_K^{HT} in the low-temperature and high-temperature regions, respectively, are proportional to the squared effective degeneracy λ of the thermally populated levels: $c_K \propto \lambda^2 - 1$. For cerium compounds with Ce^{3+} ion placed in a noncubic crystalline environment the ground multiplet splits into three doublets, thus the expected ratio is $c_K^{LT} : c_K^{HT} = 3{:}35$. In the case of $CePt_3P$, with the coefficients $c_K^{LT} = -0.063$ and $c_K^{HT} = -0.57$ yielded from linear fitting of ρ_{mag} vs log$T$ (see the dashed lines in Fig. 5(b)), the ratio is about 3:27, reasonably close to the theoretical prediction.

From the inset of Fig. 5(a), ρ drops rapidly below about 3.0 K owing to the reduction of spin-flip scattering upon entering the AFM ordered state. This magnetic transition temperature is determined from a slope change of dρ/dT in Fig. 2(b). Upon further cooling, a second slope change in ρ is observed around 1.9 K, corresponding to the pronounced kink in dρ/dT. Therefore, two magnetic transitions in $CePt_3P$ are apparent from the analysis of magnetic susceptibility $\chi(T)$, specific heat $C(T)$ and electrical resistivity $\rho(T)$, as shown in Fig. 2(b): the first transition T_{N1} corresponds to the AFM ordering temperature, while the second one T_{N2} is presumably associated with the spin reorientation. The values of T_{N1} and T_{N2} derived from different measurements agree well with each other. It is noted that while $LaPt_3P$ shows superconductivity around $T_c = 1.0$ K (from specific heat), no superconductivity is observed in $CePt_3P$ down to 0.5 K.

Considering the relativistic dispersion relation for the AFM magnon spectrum, the electrical resistivity $\rho(T)$ for $T < \Delta$ can be well described by the following equations[26,27]:

$$\rho(T) = \rho_0 + AT^2 + B_\rho\Delta^2\sqrt{\frac{T}{\Delta}}\left[1 + \frac{2}{3}\left(\frac{T}{\Delta}\right) + \frac{2}{15}\left(\frac{T}{\Delta}\right)^2\right]\exp(-\Delta/T), \tag{8}$$

where ρ_0 is the temperature-independent residual resistivity, the constant coefficient B_ρ is related to the spin-wave stiffness D by the proportionality $D^{-3/2}$ and Δ is the same gap in the spin-wave spectrum as in Eq. (5). AT^2 stems from the electron-electron scattering following the Fermi liquid theory, while the third term describes the electron-magnon scattering. This formula is applied to the electrical resistivity of $CePt_3P$ (dotted line in the inset of Fig. 5(a)) and a very good fit is obtained with the fitting parameters: $\rho_0 = 688\ \mu\Omega\cdot$cm, $\Delta = 4.0$ K, $A = 9.0\ \mu\Omega\cdot$cm/K^2 and $B_\rho = 25\ \mu\Omega\cdot$cm/K^2. Considering the relatively short fitting range of temperature, the derived Δ value for the measured polycrystalline sample is still reasonably compared with that obtained from the specific heat data.

Based on the above analyses, $CePt_3P$ displays the coexistence of three important characteristics: AFM ordering of the cerium local moments due to the Ruderman-Kittel-Kasuya-Yosida exchange interaction, the Kondo effect due to the strong 4*f* electron correlation and moderate effective 4*f*−5*d* hybridization, and the CEF interactions. The AFM ordering at $T_{N1} = 3.0$ K is clearly identified by the pronounced anomalies in the temperature-dependent magnetic, thermodynamic and electrical measurements. In addition, another anomaly at $T_{N2} = 1.9$ K is also visible from the physical properties, and is probably due to a change in the magnetic configuration within the AFM ordered phase. The behavior of $\rho(T)$ and $C(T)$ in the ordered region is well describable in terms of AFM spin-wave spectrum. The field-dependent behavior of the magnetization and electrical resistivity also indicates a MMT from the magnetic ordering to a spin-polarized state around $B_m = 3.0$ T. The magnetic structure of $CePt_3P$ is still unclear and the neutron diffraction or Mössbauer spectroscopy experiments are helpful to clarify the details of the magnetic structure.

The Kondo effect displays itself by the large value of Weiss temperature θ (compared with the ordering temperature), the reduced magnetic entropy and the specific heat jump at T_N, as well as the enhanced Sommerfeld coefficient γ_{Ce}. From the analysis of the specific heat data, the Kondo temperature T_K is estimated to be in the range of 2–6 K. Its value can be also estimated from the magnetic susceptibility as $T_K \sim |\theta|/4 \simeq 7.1$ K[30], in reasonable agreement with other estimates. Also, the Kondo effect is well manifested in the electrical resistivity for Kondo systems with strong CEF interactions which follows the negative logarithmic-temperature dependence as $\rho(T) = \rho_0 + c_k \ln T$, with Kondo coefficient $c_k < 0$[21]. The inverse susceptibility ($1/\chi(T)$) curve shows a slope change between $T = 100$–200 K which is also attributed to the CEF effect. This temperature region is in accordance with the energy scale $\Delta_1 = 240$ K of the multiplet Ce^{3+} ion estimated from the Schottky contributions of the specific heat[21,22].

Finally, it is very interesting to compare this CS compound $CePt_3P$ with the extensively studied NCS heavy fermion SC $CePt_3Si$ ($T_c = 0.75$ K)[3]. The crystal structure of $CePt_3P$ consists of alternative stacking of layers of Ce atoms and layers of distorted antiperovskite Pt_6P octahedral units along the c-axis. The Pt_6P octahedra is asymmetrically distorted perpendicular to the ab-plane but alternatively distributed in the ab-plane, resulting in a symmetric antipolar analogue of $CePt_3Si$. $CePt_3Si$ shows antisymmetric spin-orbit coupling of the platinum $5d$ electrons due to the absence of $z \rightarrow -z$ symmetry as well as mixing spin-singlet and spin-triplet pairing states. The parity mixing alone can hardly account for the heavy fermion phenomena unless the strong electron-electron correlation effects which are ensured by the presence of Ce^{3+} ions are taken into consideration together[31]. Correspondingly, the suppression of superconductivity in $CePt_3P$ may be attributed to the enhanced AFM ordering. $CePt_3P$ is, therefore, probably placed further away from the magnetic QCP compared with $CePt_3Si$ ($T_N = 2.2$ K). With an external control parameter δ, such as doping or positive pressure, the system may be shifted towards $T_N = 0$, namely the QCP[32,33]. It is thus of great interest to investigate whether superconductivity exists in $CePt_3P$ at even lower temperature than 0.5 K; if superconductivity does exist, it will provide strong evidence for the proximity to a magnetic QCP in $CePt_3P$. Comparing with $CePt_3P$, the occurrence of superconductivity at $T_c = 0.75$ K in $CePt_3Si$ implies that the NCS crystal structure may favor unconventional superconductivity within the AFM ground state.

Conclusion

In summary, we report the successful synthesis of a new compound $CePt_3P$. From the collected experimental data of magnetization, specific heat and transport measurements, this compound is characterized as an antiferromagnetic Kondo lattice with crystal electric field effect. Two successive magnetic transitions of Ce $4f$ moments are observed: the magnetic ordering at $T_{N1} = 3.0$ K and the spin reorientation at $T_{N2} = 1.9$ K. Considering the moderately enhanced Sommerfeld coefficient of $\gamma_{Ce} = 86$ mJ/mol $\cdot$ K^2 in the paramagnetic region and large value of $\gamma_0 = 247$ mJ/mol $\cdot$ K^2 in the the AFM region, the Kondo effect and the AFM order should coexist in the ground state. Thus a relatively large Fermi surface formed by the heavy quasiparticles is expected in $CePt_3P$ with a Kondo temperature $T_K \sim 2$–6 K. The ab initio crystal-field and electronic band structure calculations are necessary to further complement the present results. Further experiments such as chemical doping are presently underway in order to tune the ground state from the AFM ordering to strongly-correlated paramagnetic region.

Experimental Methods

The polycrystalline sample of $CePt_3P$ was synthesized by solid state reaction. Ce piece (99.8%), Pt powder (99.9%) and P lump (99.999%) of high purity from Alfa Aesar were used as starting materials. Firstly, CeP was pre-synthesized by reacting Ce and P at 1173 K for 72 h. Secondly, powders of CeP and Pt were weighed according to the stoichiometric ratio, thoroughly ground and pressed into pellets. The pellets were then packed in Al_2O_3 crucibles and sealed in an evacuated quartz tube which were slowly heated to 1273 K and kept at that temperature for 7 days. Finally, the samples were thoroughly ground, cold pressed and annealed in vacuum to improve the sample homogeneity. For comparison, the polycrystalline sample $LaPt_3P$ was also synthesized in the similar process. All the preparation procedures except heating were carried out in an argon protected glove box with the water and oxygen content below 0.1 ppm. The obtained $CePt_3P$ sample is less compact than $LaPt_3P$ and both of them are quite stable in the air.

Powder x-ray diffraction (XRD) measurements at room temperature were carried out on a PANalytical x-ray diffractometer (Model EMPYREAN) with a monochromatic Cu $K_{\alpha 1}$ radiation and a graphite monochromator. Lattice parameters were derived by Rietveld refinement using the program RIETAN 2000[16]. The energy dispersion x-ray spectroscopy (EDS) analysis was performed on a EDS spectrometer affiliated to a field emission scanning electron microscope (FEI Model SIRION). The electron beam was focused on a crystalline grain and the chemical compositions were averaged on at least 4 EDS spectra from different grains. The electrical resistivity $\rho(T)$ was measured by the standard four-probe method in a Quantum Design physical property measurement system (PPMS-9). The dc magnetization was measured in a Quantum Design magnetic property measurement system (MPMS-5) with the temperature range of $T = 2$-400 K. The specific heat measurements were performed in the PPMS-9 down to about 0.5 K.

References

1. Bednorz, J. G. & Müller, K. A. Possible high T_c superconductivity in the Ba-La-Cu-O system. *Z. Phys. B* **64,** 189 (1986).
2. Kamihara, Y., Watanabe, T., Hirano, M. & Hosono, H. Ion-based layered superconductor $La[O_{1-x}F_x]FeAs$ ($x = 0.05-0.12$) with $T_c = 2.6$ K. *J. Am. Chem. Soc.* **130,** 3296 (2008).
3. Bauer, E. *et al.* Heavy fermion superconductivity and magnetic order in noncentrosymmetric $CePt_3Si$. *Phys. Rev. Lett.* **92,** 027003 (2004).
4. Bauer, E. & Sigrist, M. *Non-centrosymmetric Superconductors: Introduction and Overview* (Berlin: Springer Berlin Herdelberg, 2012).
5. Frigeri, P. A., Agterberg, D. F., Koga, A. & Sigrist, M. Superconductivity without inversion symmetry: MnSi versus $CePt_3Si$. *Phys. Rev. Lett.* **92,** 097001 (2004).

6. Maisuradze, A. *et al.* Evidence for time-reversal symmetry breaking in superconducting $PrPt_4Ge_{12}$. *Phys. Rev. B* **82,** 024524 (2010).
7. Nakamura, Y. *et al.* Comparative photoemission studies on the superconducting gap of the filled skutterudite superconductors $LaPt_4Ge_{12}$ and $PrPt_4Ge_{12}$. *Phys. Rev. B* **86,** 014521 (2012).
8. Zhang, J. L. *et al.* Multiband superconductivity in $PrPt_4Ge_{12}$. *Phys. Rev. B* **87,** 064502 (2013).
9. Nishikubo, Y., Kudo, K. & Nohara, M. Superconductivity in the Honeycomb-Lattice Pnictide SrPtAs. *J. Phys. Soc. Jpn.* **80,** 055002 (2011).
10. Biswas, P. K. *et al.* Evidence for time-reversal-symmetry-broken superconductivity in locally noncentrosymmetric SrPtAs. *Phys. Rev. B* **87,** 180503(R) (2013).
11. Takayama, T. *et al.* Strong coupling superconductivity at 8.4 K in an Antiperovskite Phosphide $SrPt_3P$. *Phys. Rev. Lett.* **108,** 237001 (2012).
12. Chen, H., Xu, X. F., Cao, C. & Dai J. H. First-principles calculations of the electronic and phonon properties of APt_3P (A = Ca, Sr, and La): Evidence for a charge-density-wave instability and a soft phonon. *Phys. Rev. B* **86,** 125116 (2012).
13. Kang, C. J., Ahn, K. H., Lee, K. W. & Min, B. I. Electron and Phonon Band-Structure Calculations for the Antipolar $SrPt_3P$ Antiperovskite Superconductor: Evidence of Low-Energy Two-Dimensional Phonons. *J. Phys. Soc. Jpn.* **82,** 053703 (2013).
14. Subedi, A., Ortenzi, L. & Boeri, L. Electron-Phonon superconductivity in Apt_3P (A = Sr, Ca, La) compounds: From weak to strong coupling. *Phys. Rev. B* **87,** 144504 (2013).
15. Zocco, D. A. *et al.* Lattice dynamical properties of superconducting $SrPt_3P$ studied via inelastic x-ray scattering and density functional perturbation theory. *Phys. Rev. B* **92,** 220504 (2015).
16. Izumi, F. & Momma, K. *Solid State Phenom.* **130,** 15 (2007).
17. Szlawska, M., Kaczorowski, D., Ślebarski, A., Gulay, L. & Stepień-Damm, J. Antiferromagnetic order and Kondo-lattice behavior in single-crystalline Ce_2RhSi_3. *Phys. Rev. B* **79,** 134435 (2009).
18. Luo, Y. K. *et al.* Heavy-fermion quantum criticality and destruction of the Kondo effect in a nickel oxypnictide. *Nature Mater.* **13,** 777 (2014).
19. Balicas, L. *et al.* Magnetic field-tuned quantum critical point in $CeAuSb_2$. *Phys. Rev. B* **72,** 064422 (2005).
20. Bud'ko, S. L., Canfield, P. C., Avila, M. A. & Takabatake, T. Magnetic-field tuning of the low-temperature state of $YbNiSi_3$. *Phys. Rev. B* **75,** 094433 (2007).
21. Cornut, D. & Coqblin, B. Influence of the crystalline field on the Kondo effect of alloys and compounds with cerium impurities. *Phys. Rev. B* **5,** 4541 (1972).
22. Zlatić, V. & Monnier, R. Theory of the thermoelectricity of intermetallic compounds with Ce or Yb ions. *Phys. Rev. B* **71,** 165109 (2005).
23. Yashima, H., Mori, H., Sato, N. Satoh, T. & Kohn, K. Magnetic and nonmagnetic behavior of the Ce-Si system. *J. Magn. Magn. Mater.* **31–34,** 411 (1983).
24. Besnus, M. J., Braghta, A., Hamdaoui, N. & Meyer, A. A correlation between specific heat and the ratio T_K/T_N in magnetic Kondo lattices. *J. Magn. Magn. Mater.* **104–107,** 1385 (1992).
25. Bredl, C. D., Steglich, F. & Schotte, K. D. Specific heat of concentrated Kondo systems: (La,Ce)Al_2 and $CeAl_2$. *Z. Phys. B* **29,** 327 (1978).
26. Fontes, M. B. *et al.* Electron-magnon interaction in RNiBC (R = Er, Ho, Dy, Tb, and Gd) series of compounds based on magnetoresistance measurements. *Phys. Rev. B* **60,** 6781 (1999).
27. Yamada H. & Takada, S. Magnetoresistance due to electron-spin scattering in antiferromagnetic metals at low temperatures. *Prog. Theor. Phys.* **49,** 1401 (1973).
28. Löhneysen, H. v. *et al.* Magnetic order and transport in the heavy-fermion system $CeCu_{6-x}Au_x$. *Eur. Phys. J. B* **5,** 447 (1998).
29. Giovannini, M. *et al.* Structural chemistry, magnetism and thermodynamic. *J. Alloys Compd.* **280,** 26 (1998).
30. Hewson, A. C. in *The Kondo Problem to Heavy Fermions* (Cambridge University Press, Cambridge, England, 1993).
31. Shiroka, T. *et al.* Pairing of weakly correlated electrons in the platinum-based centrosymmetric superconductor $SrPt_3P$. *Phys. Rev. B* **91,** 245143 (2015).
32. Stewart, G. R. Non-Fermi-liquid behavior in d- and f-electron metals. *Rev. Mod. Phys.* **73,** 797 (2001); Addendum: Non-Fermi-liquid behavior in d- and f-electron metals. Rev. Mod. Phys. **78**, 743 (2006).
33. Doniach, S. The Kondo lattice and weak antireffomagnetism. Physica B + C **91,** 231 (1977).

Acknowledgements

The authors acknowledge useful discussions with Qimiao Si and Yongkang Luo. This work was supported by the Ministry of Science and Technology of China (Grants No. 2014CB921203 and 2016YFA0300402) and the National Natural Science Foundation of China (Grants No. U1332209, 11190023 and 11474082).

Author Contributions

J.C., Z.W., S.Y.Z. and C.M.F. performed the experiment(s), J.C. and Z.W. analyzed the results. J.C. and Z.A.X. designed the research and wrote the manuscript. All authors reviewed the manuscript.

Additional Information

Competing financial interests: The authors declare no competing financial interests.

How to cite this article: Chen, J. *et al.* Antiferromagnetic Kondo lattice compound $CePt_3P$. *Sci. Rep.* **7**, 41853; doi: 10.1038/srep41853 (2017).

Publisher's note: Springer Nature remains neutral with regard to jurisdictional claims in published maps and institutional affiliations.